Acta Geologica Sinica (English Edition), 2019, 93(6): 1773–1782

The Late Early Cretaceous Mo Mineralization in the South China Mo Province: Constraints from U–Pb and Re–Os Geochronology of the Lufeng Porphyry Mo Deposit

WANG Yongbin[1, 2, *], ZENG Qingdong[1, 2, 3], LIU Jianming[1, 2, 3] and ZHOU Lingli[1, 2]

[1] *Key Laboratory of Mineral Resources, Institute of Geology and Geophysics, Chinese Academy of Sciences, Beijing 10029, China*
[2] *Institutions of Earth Science, Chinese Academy of Sciences, Beijing 100029, China*
[3] *College of Earth and Planetary Science, University of Chinese Academy of Sciences, Beijing 100049, China*

Abstract: Compared to other Mo provinces, few studies focused on the South China Mo Province (SCMP), especially for Early Cretaceous Mo mineralization. The Lufeng porphyry Mo deposit in the SCMP is characterized by disseminated and veinlet-type mineralization in granite porphyry, gneiss, and rhyolite. In this study, six molybdenite samples yield a Re–Os isochron age of 108.0±1.8 Ma, which is consistent with the zircon U–Pb age of the granite porphyry (108.4±0.8 Ma). The coincidence of magmatic and hydrothermal activities indicates that Mo mineralization was associated with the intrusion of granite porphyry during the late Early Cretaceous. A compilation of U–Pb and Re–Os chronological data suggests that an extensive and intensive Mo mineralization event occurred in the SCMP during the late Early Cretaceous. The marked difference in molybdenite Re contents between Cu-bearing (85–536 ppm) and Cu-barren (1.3–59 ppm) Mo deposits of the late Early Cretaceous indicates that the ore-forming materials were derived from strong crust–mantle interactions. Together with regional petrological and geochemical data, this study suggests that late Early Cretaceous Mo mineralization in the SCMP occurred in an extensional setting associated with the roll-back of the Paleo-Pacific slab.

Key words: U–Pb, Re–Os, porphyry Mo deposit, Lufeng, South China Mo Province

Citation: Wang et al., 2019. The Late Early Cretaceous Mo Mineralization in the South China Mo Province: Constraints from U–Pb and Re–Os Geochronology of the Lufeng Porphyry Mo Deposit. Acta Geologica Sinica (English Edition), 93(6): 1773–1782. DOI: 10.1111/1755-6724.14365

1 Introduction

China has the largest molybdenum resource worldwide, with most being concentrated in six Mo provinces, including the Northeast China, Yanliao, Qinling-Dabie, Middle-Lower Yangtze River Valley, South China, and Sanjiang (Fig. 1a. Zeng et al., 2013; Chen et al., 2017; Li et al., 2017; Ni et al., 2017a, b). The South China Mo Province (SCMP) hosts at least 35 Mo deposits with a total resource of ~0.3 Mt Mo metal that accounting for ~2.5% of China's total Mo resources (Zeng et al., 2013). The NE–SW-trending SCMP includes the Cathaysia Block and the southeastern margin of the Yangtze Craton (Mao et al., 2013; Wang et al., 2017). Ages of these Mo deposits span from the Early Paleozoic to the Late Mesozoic, with most being in the Late Mesozoic (Zhong et al., 2017). In particular, more and more recent discoveries call for further studies for Early Cretaceous Mo mineralization, which will be helpful to understand the regional mineralization regularity and the background of tectonic setting.

The Lufeng porphyry Mo deposit in the SCMP, also known as Lingjiao Mo deposit, is located in Zhejiang Province, South China, and was discovered sixty years ago. Previous studies focusing on geological features indicate that Mo mineralization is associated mainly with ore-bearing granite porphyry (Wu and Yang, 1999). However, owing to a lack of geochronological studies, the genetic link between mineralization and magmatism is unclear. The molybdenite Re–Os and zircon U–Pb dating provide robust geochronometers, reliably constraining the timing of magmatism and mineralization (Stein et al., 1997) and improving understanding of such genetic links. In this study, we present secondary-ion mass spectrometry (SIMS) zircon U–Pb ages for the granite porphyry and inductively coupled plasma-mass spectrometry (ICP–MS) molybdenite Re–Os ages for the Lufeng Mo deposit, with the aims of revealing genetic relationships between hydrothermal and magmatic activities and characterizing the geodynamic setting that controlled regional Mo mineralization.

2 Regional Geology

The South China Block (SCB) is separated from the North China Craton (NCC) by the Qinling–Dabie Orogenic Belt (Fig. 1a). The SCB was formed initially through amalgamation of the Yangtze Craton and Cathaysia Block along the Jiangshan–Shaoxing Fault during late Neoproterozoic (Fig. 1b. Chen et al., 1991;

* Corresponding author. E-mail: wangyongbin@mail.iggcas.ac.cn

© 2019 Geological Society of China

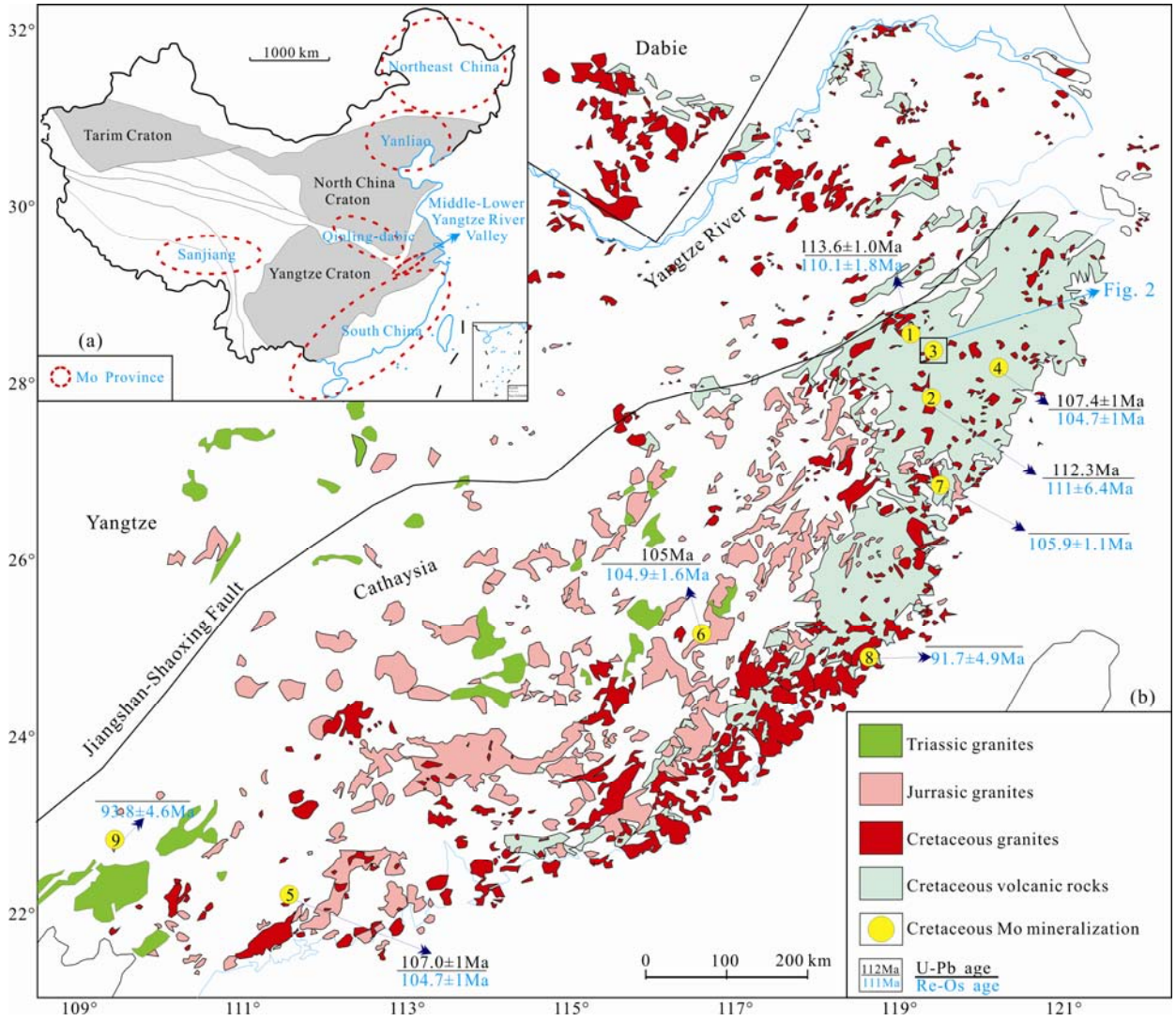

Fig. 1. (a) Distribution map of Mo metallogenic province in China (adapted from Zeng et al., 2013. China basemap after China National Bureau of Surveying and Mapping Geographical Information); (b) simplified geological map of South China Mo Province showing the distribution of the Mesozoic granitoid and volcanic rocks and Early Cretaceous Mo mineralization (after Wang et al., 2016 and Wang et al., 2017).

1–Zhilingtou Mo-PbZn-AuAg; 2–Sanzhishu Mo; 3–Lufeng Mo; 4–Shipingchuan Mo; 5–Shilu Cu-Mo; 6–Luoboling Cu-Mo; 7–Chilu Mo; 8–Lishan Mo; 9–Wangshe Mo-Cu

Zheng et al., 2013; Xu et al., 2014; Zhao et al., 2018), with extensive Paleozoic rocks unconformably overlying the Proterozoic metamorphic basement (Shu and Charvet, 1996; Mei et al., 2017; Hu et al., 2018). The SCB then collided with the NCC during the Early Triassic (Zhou et al., 2006), and northwestward subduction of the Paleo-Pacific Plate beneath the SCB probably occurred during the Early Jurassic (Zhou and Li, 2000). The widespread Cretaceous magmatic association of A-type granite, syenite, gabbro and bimodal volcanic rocks (Chen et al., 2002; Wang et al., 2006; Li and Li, 2007) likely developed in a continental back-arc extension setting due to roll-back of the Paleo-Pacific Plate (Zhou et al., 2006).

During the Mesozoic, SE China was characterized by widespread and intensive magmatic activities, forming a volcanic–intrusive belt covering more than 220,000 km^2 (Fig. 1b. Zhou et al., 2006). Over 90% of the magmatic rocks are granites or equivalent volcanic rocks; gabbro and basalt are rare, and diorite and andesite even more so. Most of the Triassic magmatic rocks are found in the southern SCB and only as dispersed small plutons barren of Mo mineralization (Zhu et al., 2013). Late Mesozoic large-scale igneous rocks are widely exposed in the Zhejiang, Fujian, Jiangxi and Guangdong provinces in SE China, grouped in the Jurassic (180–145 Ma) and Cretaceous (145–90 Ma) periods (Zhou and Li, 2000). An obvious younging trend toward the coast is apparent (Fig. 1b). Jurassic magmatism throughout the western SCB is dominated by peraluminous S-type granites with minor I-type granites (Li et al., 2018; Wang et al., 2018). Cretaceous magmatism produced mainly high-K I-type and A-type granites along the coast (Wang et al., 2016).

3 Geology of the Lufeng Mo Deposit

3.1 Ore geology

The Lufeng Mo deposit is located in the northern Cathaysia Block and is part of the SCMP (Fig. 1b). Rocks exposed in the mining area include those of Badu group and Dashuang group (Fig. 2a). The basement Badu group comprises amphibolite-facies gneiss and migmatites (Fig. 3a. Pirajno et al., 1997; Li et al., 2010), which generally strike NE and dip SW at 65°–75°. Felsic gneisses and migmatites yield zircon U–Pb ages of 1.9–1.7 Ga (Gan et al., 1995). The cover rocks of the Dashuang group are composed of Late Jurassic rhyolite (Fig. 3b), dipping to SE at 60°–70°.

Faults are common and well developed in the ore district, (Fig. 2a) and trend mainly NE and NW. Four NE-striking faults have lengths of 1–2 km and dip at 40°–45°. NW-striking faults at 280°–340° cut the early NE-striking faults and ore body.

Intermediate-acidic intrusive rocks, including Triassic granodiorite and Early Cretaceous granite porphyry, are distributed in the mining area (Fig. 2a). The granodiorite is gray in color and porphyritic in texture. Phenocrysts (35–45 vol%) are predominantly plagioclase and K-feldspar. The matrix comprises plagioclase (35–45 vol%), K-feldspar (15–25 vol%), quartz (10–15 vol%), biotite and hornblende (5–10 vol%), and accessory minerals such as zircon and apatite. The granite porphyry of the Lufeng Mo

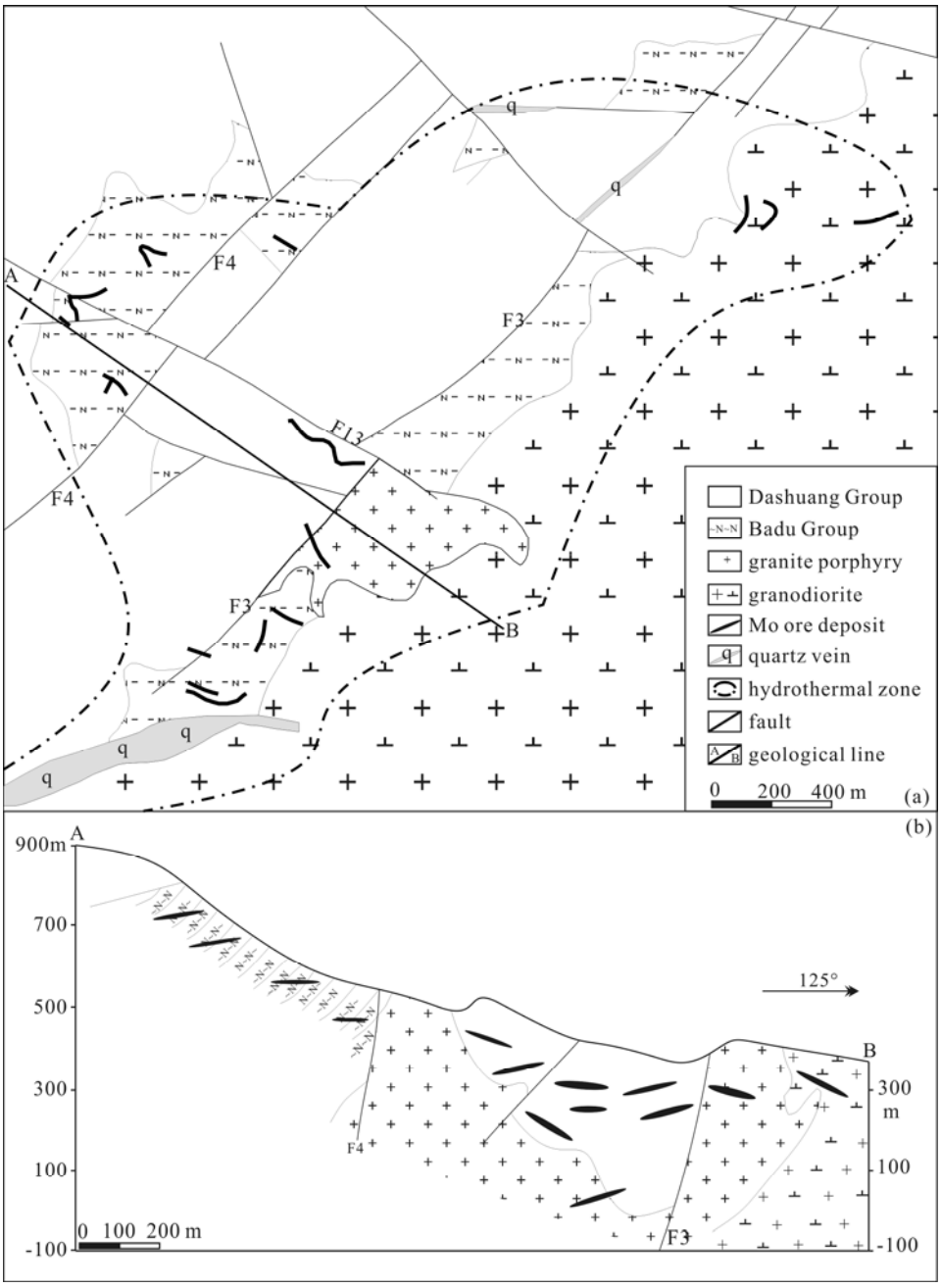

Fig. 2. (a) Simplified geological map of the Lufeng Mo deposit; (b) simplified geological cross-section AB exploration line of the Lufeng Mo deposit (after Wu and Yang, 1999).

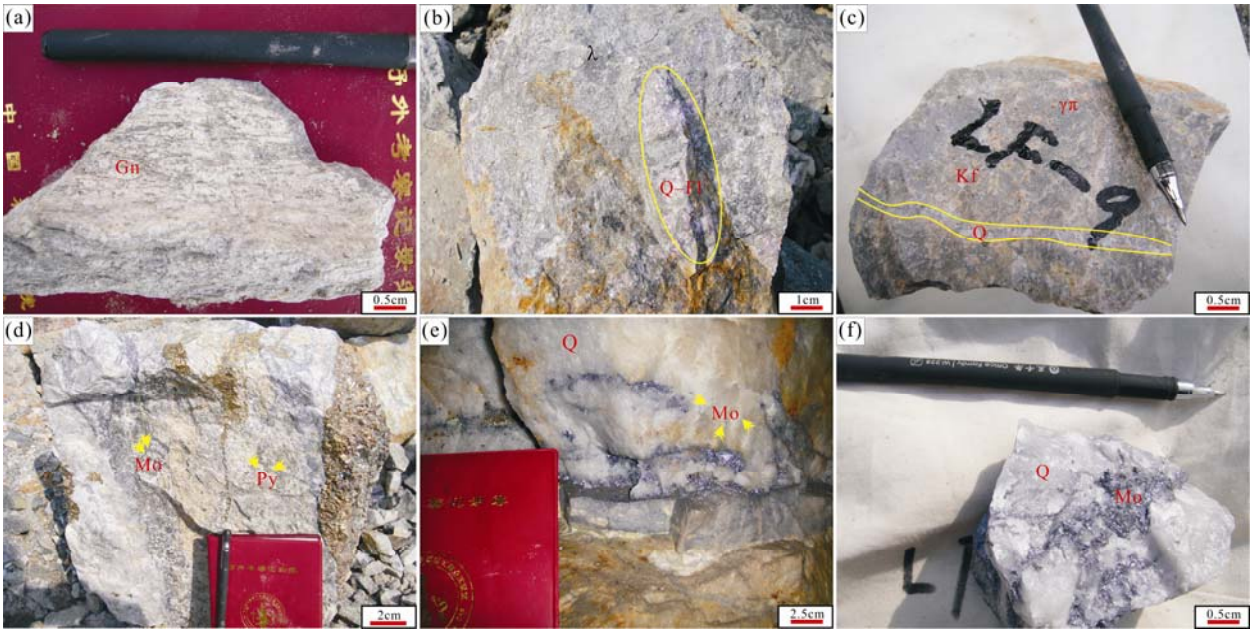

Fig. 3. The photographs of Mo mineralization and wall rock from Lufeng Mo deposit.
(a) Altered gneiss; (b) mineralized rhyolite and Stage III, quartz-fluorite-calcite mineral assemblages; (c) Granite porphyry and Stage I, quartz ± molybdenite vein with potassic and silicic alteration; (d) Stage II, quartz-molybdenite-pyrite veinlet with the silicic, sericitic and cloritic alteration; (e) quartz-molybdenite vein with the silicic and sericitic alteration in granite porphyry; (f) quartz-molybdenite sample used for Re-Os dating. Gn–Gneiss; λ–rhyolite; γπ–Granite porphyry, Kf–K-feldspar; Ser–Sericite; Q–Quartz; Fl–Fluorite; Mo–Molybdenite; Py–Pyrite.

district is closely associated with the Mo mineralization. This porphyry is red in color and is medium- to fine-grained (Fig. 3c), with phenocrysts being mainly K-feldspar and quartz, and a light mineral assemblage of K-feldspar, plagioclase, and quartz constituting more than 95 vol% of the rock.

3.2 Orebodies and hydrothermal alteration

Mo mineralization occurs chiefly within the granite porphyry but also in the Mesoproterozoic gneiss and Late Jurassic rhyolites (Figs. 2a and 2b). Eleven individual orebodies have been identified in the Lufeng Mo district, although only four (Nos. IV, VII, X and XI) have been mined. The orebodies are generally vein-like and lenticular.

Orebody IV comprises several small ore veins clustered in the Mesoproterozoic gneiss. The veins are lenticular with lengths of 130–230 m and depths of 0.1–2 m, generally striking 55°–105° and dipping at 18°–25°. Orebody VII contains NS-striking veins in the Mesoproterozoic gneiss. This orebody has a shallow mineralization zone more than 150 m long and dips W at 20°. Orebody X includes ore veins in the Jurassic rhyolites. These veins are 150–230 m long and 0.3–0.8 m deep. They generally strike 100°–110° and dip NE at 20°–47°. The orebody XI occurs in the southeastern part of orebody X, and is similar to the latter in terms of striking and dipping.

The major types of hydrothermal alteration within wall rocks of the Lufeng Mo deposit are feldspathization, silicification, sericitization, chloritization, kaolinitization, carbonatization and fluoritization. Alteration zonation has not been distinguished owing to overlapping previous alteration and limited exposures. Alteration within the granite porphyry comprises mainly potassic, silicic, and sericitic hydrothermal alterations, whereas, the gneiss and rhyolites are characterized by silicification, sericitization, chloritization, kaolinitization and carbonatization. Both macro- and micro-scale observations indicate that molybdenite and pyrite occur mostly in quartz veins or are disseminated in wall rocks. Mo mineralization is closely associated with potassic and phyllic alteration.

The Mo occurs mainly as molybdenite–quartz veins in veinlets or stockwork, or as disseminated Mo within the altered intrusion. The dominant ore minerals in the Lufeng deposit are molybdenite and pyrite (Fig. 3d). The gangue minerals include quartz, sericite, muscovite, chlorite, epidote, calcite, and minor fluorite (Figs. 3b and 3c). Based on the cross-cutting relationships of veins, the occurrence of mineral assemblages, and the types of hydrothermal alteration, the mineralization process can be divided into three stages: (I) The early stage of weak and disseminated Mo mineralization in the granite porphyry, marked by a molybdenite–K-feldspar–quartz assemblage (Fig. 3c); (II) the main stage of quartz–molybdenite–pyrite veinlets or molybdenite films occurring in the fractures (Fig. 3e); and (III) the late stage including quartz–calcite–fluorite mineral assemblages and traces of pyrite (Fig. 3b).

4 Samples and Methods

4.1 Sample description

The granite porphyry (sample LF–9) was collected for SIMS zircon U–Pb dating. This sample is characterized by intense silicification and has an inequigranular porphyritic texture (Fig. 3c). The phenocrysts (30–40 vol%) are

mainly K-feldspar and quartz. The matrix consists of quartz, K-feldspar, plagioclase, biotite, and accessory minerals such as zircon, apatite, and magnetite. Zircons were separated from crushed subsamples, and well-formed prismatic zircons with few cracks and inclusions were hand-picked under a binocular microscope.

Six molybdenite samples were collected from quartz–molybdenite veinlets of the main ore bodies (samples LF–2 to LF–8). Fresh molybdenite samples were hand-picked to ensure >99% purity, and 0.5–1.0 g separates were crushed to approximately 0.1 mm for analysis.

4.2 SIMS U–Pb dating

The zircon grains for U–Pb analysis, together with the zircon standards Plesovice and Qinghu were mounted in epoxy mounts which were then polished to approximately half the width of the crystals for analysis. All zircons were documented with transmitted and reflected light photomicrographs and cathodoluminescence (CL) images to reveal their internal structures. The mounts were vacuum-coated with high-purity gold prior to secondary ion mass spectrometry (SIMS) analysis.

Measurements of U, Th and Pb were conducted using the Cameca IMS-1280 SIMS at the Institute of Geology and Geophysics, Chinese Academy of Sciences in Beijing. Analytical procedures are similar to those described by Li et al. (2009). The O_2^- primary ion beam was accelerated at 13 kV, with an intensity of ca. 8 nA. The ellipsoidal spot was approximately 20×30 μm in size. Positive secondary ions were extracted with a 10 kV potential. Oxygen flooding was used to increase the O_2 pressure to ca. 5 ppm Torr in the sample chamber, enhancing the secondary Pb^+ sensitivity by a factor of > 2 to a value of ca. 24–28 cps/nA/ppm for zircon.

In the secondary ion beam optics, a 60 eV energy window was used, together with a mass resolution of ca. 5400, to separate Pb^+ peaks from isobaric interferences. Precise mass calibration was maintained by using an automatic routine in the Cameca CIPS software to scan over large peaks and extrapolate the mass to B-field curve for peaks between these reference points (Whitehouse et al., 1999). A single electron multiplier was used in ion-counting mode to measure secondary ion beam intensities by peak jumping. Each measurement consisted of 7 cycles, and the total analytical time was ca. 12 min.

Pb/U calibration was performed relative to the 1065 Ma standard zircon 91500 with Th and U concentrations of ca. 29 and 81 ppm, respectively (Wiedenbeck et al., 1995). Analyses of the standard zircon 91500 were interspersed with unknown grains. The measured compositions were corrected for common Pb using non-radiogenic ^{204}Pb. The uncertainties in individual analyses in the data tables are reported at all levels, and the mean ages of the pooled U/Pb (and Pb/Pb) analyses are reported at the 95% confidence interval. Data reduction was carried out using the Isoplot/Ex v. 3.00 program (Ludwig, 2003).

4.3 ICP–MS Re–Os dating

Re–Os isotope analysis was carried out at the National Research Center of Geoanalysis, Chinese Academy of Geological Sciences, Beijing. Molybdenite was dissolved and equilibrated with ^{185}Re and ^{190}Os spikes. Osmium was distilled as OsO_4 from an H_2SO_4–$Ce(SO_4)_2$ solution, and separation of rhenium from the remaining solution was achieved by solvent extraction and cation exchange resin chromatography. Re and Os concentrations were determined by the isotopic dilution method using an ICP–MS (TJA X–series) made by the Thermo Electron Corporation in the USA. The analytical procedures follow those of Du et al. (1995, 2007), and Qu and Du (2003). During the course of the analyzed, blanks were Re < 0.041 ppb and ^{187}Os< 0.0002 ppb, which are far lower than the Re and Os concentrations in the samples analyzed. The Re–Os isochron was calculated and plotted by Isoplot 3.0 (Ludwig, 2003). Re–Os model ages were calculated following the equation $t = [\ln(1+{}^{187}Os/{}^{187}Re)]/\lambda$, where λ denotes the decay constant of ^{187}Re and t is the age. The ^{187}Re decay constant is 1.666×10^{-11} a^{-1}, with an uncertainty of 0.31% (Smoliar et al. 1996). The uncertainty of the Re–Os ages is reported as 2σ. The uncertainty in the model age is derived from the uncertainty in the decay constant (1.02%), with a confidence level of 95%.

5 Results

5.1 Zircon U–Pb dating

The zircons from granite porphyry sample LF–9 are mostly euhedral, prismatic, transparent, and colorless, with lengths of 100–250 μm and aspect ratios of 1:1–1:4. In the cathodoluminescence images, most zircons display simple euhedral oscillatory zoning consistent with single-generation growth and a magmatic origin (Hoskin and Schaltegger, 2003; Wu and Zheng, 2004).

U–Pb age results are presented in Table 1 and Fig. 4. Seventeen analyses were conducted on 17 zircons from the sample LF–9. The zircon U and Th contents are 292–1393 ppm and 142–1457 ppm, respectively, with Th/U ratios of 0.19–1.76. The common-Pb content is generally low (<1% of $f^{206}Pb$) in this analysis. $^{206}Pb/^{238}U$ and $^{207}Pb/^{235}U$ ratios are internally consistent within analytical precision and yield a concordant age of 108.4±0.8 Ma (MSWD=0.4) (Fig. 4a), with a weighted-mean $^{206}Pb/^{238}U$ age of 108.4±0.9 Ma (MSWD=0.3) (Fig. 4b), which is the best estimate of the crystallization age of sample LF–9.

5.2 Molybdenite Re–Os dating

Re–Os dating results for six molybdenite samples are listed in Table 2. Total Re contents are 4.0–10.7 ppm, and the range of ^{187}Re and ^{187}Os contents yielded an isochron age of 108±1.8 Ma with an initial ^{187}Os content of 0.1±0.1 ppb (MSWD=0.3) (Fig. 5a). The Re–Os model ages of the six samples have a narrow range of 106.5–107.7 Ma (Fig. 5b) with a weighted-mean age of 107.1±0.6 Ma. The isochron age is consistent with this weighted mean age within error and likely represents the age of Mo mineralization in the Lufeng Mo deposit.

6 Discussions

6.1 Geochronology of magmatism and mineralization

Mo mineralization in the Lufeng deposit occurs mainly

Table 1 SIMS U–Pb Zircon data of the granite porphyry from the Lufeng Mo deposit

No.	Th/ppm	U/ppm	Th/U	f^{206}Pb (%)	Isotopic ratios						Age (Ma)					
					$^{207}Pb/^{206}Pb$	±σ	$^{207}Pb/^{235}U$	±σ	$^{206}Pb/^{238}U$	±σ	$t_{207/206}$	1σ	$t_{207/235}$	1σ	$t_{206/238}$	1σ
LF-9-1	1316	1113	1.18	0.04	0.04869	1.62	0.11424	2.23	0.0170	1.54	132.7	37.6	109.8	2.3	108.8	1.7
LF-9-2	1264	1116	1.13	0.04	0.04890	2.27	0.11631	2.73	0.0173	1.51	142.8	52.4	111.7	2.9	110.3	1.7
LF-9-3	341	729	0.47	0.91	0.04501	3.81	0.10574	4.10	0.0170	1.51	-55.4	90.4	102.1	4.0	108.9	1.6
LF-9-4	142	732	0.19	0.00	0.04788	2.49	0.11195	2.94	0.0170	1.56	93.5	58.0	107.7	3.0	108.4	1.7
LF-9-5	1191	1178	1.01	0.00	0.04826	1.57	0.11516	2.17	0.0173	1.50	112.0	36.5	110.7	2.3	110.6	1.6
LF-9-6	998	806	1.24	0.12	0.04952	2.44	0.11491	2.88	0.0168	1.52	172.4	56.0	110.4	3.0	107.6	1.6
LF-9-7	1457	1146	1.27	0.04	0.04801	1.58	0.11271	2.18	0.0170	1.51	100.0	36.9	108.4	2.2	108.8	1.6
LF-9-8	515	292	1.76	0.15	0.04755	3.14	0.11071	3.50	0.0169	1.55	77.0	73.0	106.6	3.5	107.9	1.7
LF-9-9	386	546	0.71	0.00	0.04781	2.30	0.11190	2.75	0.0170	1.50	90.0	53.7	107.7	2.8	108.5	1.6
LF-9-10	574	678	0.85	0.03	0.04787	2.04	0.11212	2.54	0.0170	1.50	92.7	47.7	107.9	2.6	108.6	1.6
LF-9-11	251	908	0.28	0.10	0.04804	1.98	0.11083	2.48	0.0167	1.50	101.1	46.1	106.7	2.5	107.0	1.6
LF-9-12	514	629	0.82	0.00	0.04915	2.11	0.11359	2.59	0.0168	1.51	155.1	48.6	109.2	2.7	107.2	1.6
LF-9-13	433	617	0.70	0.00	0.04949	2.86	0.11588	3.24	0.0170	1.53	171.1	65.4	111.3	3.4	108.6	1.6
LF-9-14	468	677	0.69	0.00	0.04688	2.05	0.10943	2.58	0.0169	1.56	43.0	48.3	105.4	2.6	108.2	1.7
LF-9-15	1070	904	1.18	0.00	0.04950	1.74	0.11612	2.30	0.0170	1.51	171.6	40.0	111.5	2.4	108.8	1.6
LF-9-16	459	663	0.69	0.06	0.04772	2.74	0.10993	3.14	0.0167	1.54	85.4	63.7	105.9	3.2	106.8	1.6
LF-9-17	1454	1393	1.04	0.00	0.04974	1.39	0.11649	2.05	0.0170	1.50	183.0	32.1	111.9	2.2	108.6	1.6

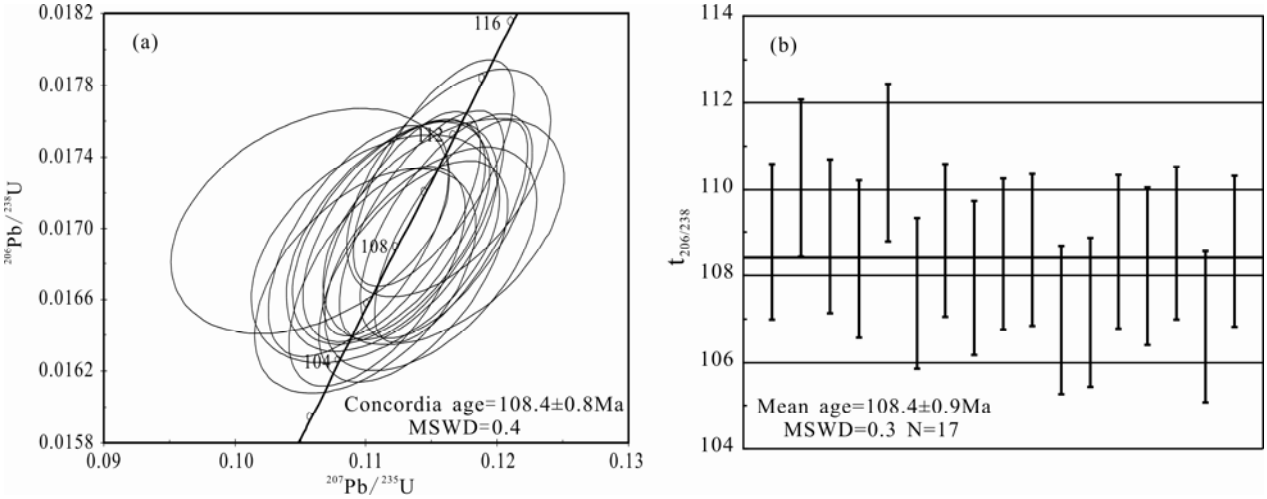

Fig. 4. SIMS U–Pb concordia diagram of zircons from granite porphyry in the Lufeng Mo deposit.

Table 2 Re–Os isotope data for molybdenite samples the Sanzhishu porphyry Mo deposit

Sample	Brief sample description	Weight (g)	Re (ppm)		^{187}Re (ppm)		^{187}Os (ppb)		Model age (Ma)	
			Measured	2σ	Measured	2σ	Measured	2σ	Measured	2σ
LF-2	Quartz-molybdenite vein	0.10101	6.85	0.05	4.30	0.03	7.69	0.07	107.1	1.5
LF-4	Quartz-molybdenite vein	0.10078	6.24	0.06	3.92	0.04	7.03	0.06	107.5	1.6
LF-5	Quartz-molybdenite vein	0.10295	6.51	0.06	4.09	0.04	7.30	0.06	107.0	1.6
LF-6	Quartz-molybdenite vein	0.10018	10.70	0.09	6.73	0.06	12.02	0.10	107.1	1.5
LF-7	Molybdenite-quartz vein	0.0649	4.00	0.03	2.51	0.02	4.46	0.04	106.5	1.5
LF-8	Molybdenite in the granite	0.10062	6.88	0.07	4.32	0.04	7.76	0.07	107.7	1.6

Notes: All the data are calculated using the decay constant λ (^{187}Re) = 1.666×10^{-11}/a (Smoliar et al., 1996); uncertainties are absolute at 2σ with error on Re and ^{187}Os contents and the uncertainty in the ^{187}Re decay constant.

as disseminations or veinlets within the ore-bearing granite porphyry. The feldspathization, silicification, sericitization, chloritization, kaolinitization, carbonatization and fluoritization, are particularly intense around the granite porphyry, demonstrating a spatial relationship between Mo mineralization and granite porphyry. The multiple stages of mineralization and hydrothermal alteration identified indicate several stages of hydrothermal-fluid activity. The calculated isochron molybdenite Re–Os (108±1.8 Ma) and zircon U–Pb (108.4±0.8 Ma) ages likely indicate the timings of Mo mineralization and granite porphyry crystallization, respectively. The spatio-temporal relationship between Mo mineralization and granite porphyritic magma crystallization suggests that the Lufeng Mo mineralization was genetically related to the intrusion of the granite porphyry during the late Early Cretaceous.

The late Early Cretaceous Mo mineralization has been previously reported in the SCMP (Table 3), including the Sanzhishu Mo (111±6.4 Ma; Wang et al, 2017) Zhilingtou Mo–Pb–Zn–Au–Ag (113±2.4 Ma; Zeng et al., 2012), Shipingchuan Mo (104.7±1 Ma; Wang et al., 2013), Shilu Cu–Mo (104.7±1 Ma; Zhao et al., 2012), Luoboling Cu–Mo (104.9±1.6 Ma; Liang et al., 2012), Chilu Mo

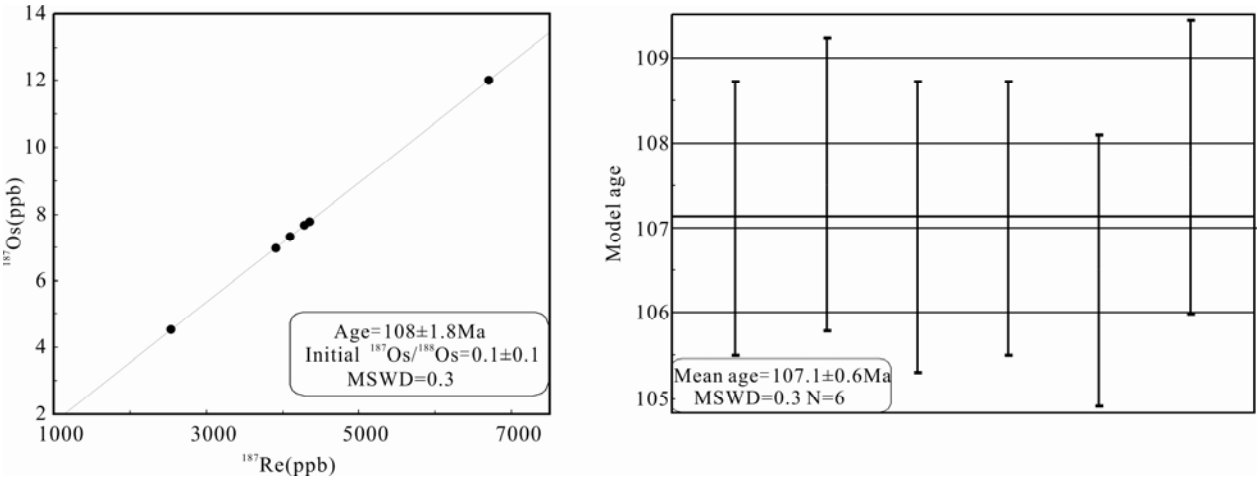

Fig. 5. Re–Os isochron plot for molybdenite samples from the Lufeng deposit.

Table 3 The characteristics of late Early Cretaceous Mo deposits in the SCMP

No.	Deposit	Deposit type	Commodity	Host rocks	Ore texture	Ore-forming intrusions (Ma)	Mineralization age (Ma) /Re (ppm)	Ore minerals	Gangue minerals	References
1	Zhilingtou	Porphyry	Mo-PbZn-AuAg	Proterozoic genesis, Granite porphyry	Diss, Sw, Br	Granite porphyry (113.6±1.0)[1]	110.1±1.8/ 15–59	Py, Mo, Sp, Gn	Qtz, Ser, Fl, Cal, Chl	Zeng et al. 2012
2	Sanzhishu	Porphyry	Mo	Proterozoic genesis, Monzogranite	Diss, Sw	Monzogranite (112.3)[1]	111±6.4/ 16–26	Mo, Py	Qtz, Ser, Fl, Cal, Chl	Wang et al., 2017
3	Lufeng	Porphyry	Mo	Proterozoic genesis, Rhyolite, Granitic porphyry	Diss, Sw	Granite porphyry (108.4±0.8)[1]	108±1.8/ 4–10.7	Mo, Py	Qtz, Ser, Fl, Cal, Chl	This study
4	Shipingchuan	Quartz-vein	Mo	Crystal tuff, orthophyre	Diss, Sw	orthophyre (107.4±1.0)[1]	104.7±1/ 1.3–45.6	Mo, Py	Qtz, Ser, Fl	Wang et al., 2013
5	Shilu	Skarn	Cu-Mo	Carboniferous carbonate, Granodiorite	Diss, Sw	Granodiorite (107±1)[2]	104.7±1/ 85–536	Mo, Ccp, Py	Qtz, Di, Grt, Ser, Chl	Zheng et al., 2015; Zhao et al., 2012
6	Luoboling	Porphyry	Cu-Mo	Granodiorite	Diss, Sw	Granodiorite (105)[3]	104.9±1.6/ 112–237	Mo, Ccp, Py	Qtz, Ser, Kf	Zhang et al., 2001; Liang et al., 2012
7	Chilu	Porphyry	Mo	Rhyolite, Granite, Monzogranite	Diss, Sw	Granite	105.9±1.1/ 8–16	Mo, Py	Qtz, Ser, Kf	Zhang et al., 2009
8	Lishan	Porphyry	Mo	Quartz diorite, Rhyolitic porphyry	Diss, Sw	Granite porphyry	91.7±4.9/ 14–23	Mo, Py	Qtz, Ser, Kf, Fl, Kao	Wang et al., 2009
9	Wangshe	Porphyry	Mo-Cu-W	Biotite granite	Diss, Sw	Biotite granite	93.8±4.6/ 23–33	Mo, Ccp, Wf, Py	Qtz, Ser, Kf, Fl, Kao	Lin et al., 2008

Notes: Ore-forming intrusion age determination: [1]SIMS U–Pb; [2]LA-ICP-MS U–Pb; [3]ICP-MS Rb–Sr. All mineralization ages were obtained by Re-Os isochron dating. Ore textures: Diss, disseminated; Sw, stockwork; Br, breccia. Mineral obbreviations: Chl, Chlorite; Kao, Kaolinite; Kf, K-feldspar; Ser, Sericite; Fl, Fluorite; Cal, Calcite; Di, Diopside; Grt, Garnet; Mo, Molybdenite; Py, Pyrite; Sp, Sphlerite; Gn, Galena; Ccp, chalcopyrite; Wf, wolframite.

(105.9±1.1 Ma; Zhang et al., 2009), Lishan Mo (91.7±4.9 Ma; Wang et al., 2009) and Wangshe Mo–Cu–W (93.8±4.6 Ma; Lin et al., 2008) deposits. Our geochronological study confirms the occurrence of extensive late Early Cretaceous magmatic–hydrothermal Mo mineralization in the SCMP (Fig. 6).

6.2 Re contents of molybdenite

The Re content of molybdenite has previously been applied as an indicator of sources of ore-forming materials (Mao et al., 1999; Stein et al., 2001). In a comparison of Re contents of molybdenite from different types of endogenic Mo deposits in China, Mao et al. (1999) found that Re content of molybdenite decreases progressively from mantle source (hundreds of ppm), to mixed source of mantle and crustal materials (tens of ppm) to crust source (several ppm). Deposits involving mantle magma underplating or melting of mafic and ultramafic rocks usually have high molybdenite Re contents, whereas, deposits originating from continental crust or sedimentary sequences poor in organic matter have lower Re contents (Stein et al., 2001). The Lufeng Mo deposit has low molybdenite Re contents (4–10.7 ppm), indicating that the ore-forming materials were derived predominantly from the crust source (Fig. 7). However, molybdenite Re contents of other late Early Cretaceous Mo deposits in the SCMP vary widely (1.3–536 ppm; Fig. 7) and are correlated with Cu content. Re contents of Cu-bearing Mo deposits such as the Shilu and Luobuling deposits are 85–536 ppm, suggesting that the ore-forming materials were derived from mantle source, whereas Cu-barren Mo deposits have Re contents of 1.3–59 ppm, indicating a crust source. This marked difference between Cu-bearing and Cu-barren Mo deposits was also reported for Mo

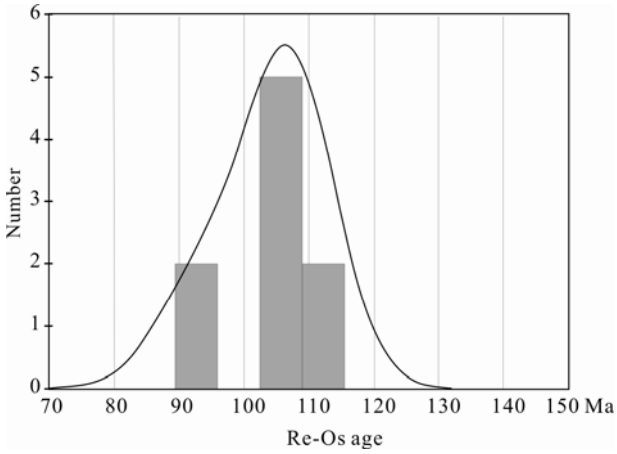

Fig. 6. Cumulative probability plot of isotopic ages for the late Early Cretaceous Mo deposits in the SCMP.

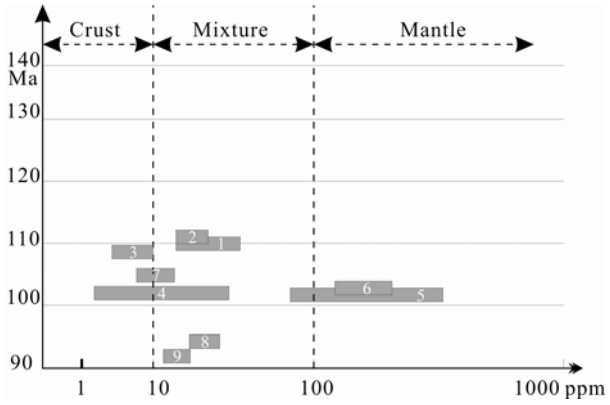

Fig. 7. Distribution of molybdenite Re contents of the late Early Cretaceous Mo deposits in the SCMP.

deposits in Mongolia and Russia (Berzina et al., 2005). The typically differing Re contents of Cu-bearing and coeval Cu-barren Mo deposits indicate intense crust–mantle interaction, which provided ore-forming materials for the late Early Cretaceous Mo deposits in the SCMP.

6.3 Geodynamic setting

Widespread A-type granites (Qiu et al., 2004; Chen et al., 2013) and the development of pull-apart basins filled with bimodal volcanic rocks (Zhou et al., 2006) suggest that SE China was in an extensional setting during the Early Cretaceous. Wang et al. (2017) reported that Cretaceous Mo mineralization in the SCMP mainly occurred during two episodes: the early Early Cretaceous (130–145 Ma) and the late Early Cretaceous (90–120 Ma). Most of the Mo mineralization occur in the latter episode, which requires detailed examination of the genesis to understand the regional mineralization regularity and the background of tectonic setting.

The early Early Cretaceous A-type granitic rocks occur inland and have bulk-rock $\varepsilon_{Nd}(t)$ values of −6.5 to −3.6 and zircon $\varepsilon_{Hf}(t)$ values of −7.8 to −0.9, with Mesoproterozoic T_{DMC} ages for both Nd and Hf isotopes (Yang et al., 2012). However, the late Early Cretaceous A-type granitoids in the coastal areas have higher $\varepsilon_{Nd}(t)$ values of −10.8 to −0.7 and $\varepsilon_{Hf}(t)$ values of −11.6 to +4.5 (Liu et al., 2012; Li et al., 2014). These differences suggest that the regional extension stress field migrated from inland to the coast. Moreover, Wang et al. (2017) has suggested that the increase in Re contents from the early (130–145 Ma) to late (120–90 Ma) Mo mineralization periods in the SCMP, indicates crust–mantle magma mixing during lithospheric extension in the late mineralization period. Here the marked differences in molybdenite Re contents between Mo–Cu deposits (85–536 ppm) and Mo-dominated deposits (1.3–59 ppm) suggests strong crust–mantle magma interaction. Together, the features imply progressive involvement of the mantle in enhanced lithospheric extensional tectonic setting from the early to late Early Cretaceous.

Taking all these considerations into account, this is most likely attributed to progressive slab roll-back of the Paleo-Pacific Plate (Jiang et al., 2011; Wang et al., 2017), which may have triggered intense tectono–magmatic–hydrothermal activity in the coastal area of SE China. With ongoing extension during slab roll-back, the crust and lithospheric mantle progressively thinned, with asthenospheric upwelling initiating partial melting of crustal rocks and generating late Early Cretaceous granitic magmas and extensive Mo mineralization in the SCMP.

7 Conclusions

(1) Together with previously reported geochronological data, Zircon SIMS U–Pb (108.4±0.8 Ma) and molybdenite ICP-MS Re–Os (108±1.8 Ma) ages of the Lufeng porphyry Mo deposit confirm extensive late Early Cretaceous magmatic–hydrothermal Mo mineralization in the SCMP.

(2) The substantial difference in molybdenite Re contents between Cu-bearing (85–536 ppm) and Cu-barren (1.3–59 ppm) Mo deposits suggests that crust–mantle interaction was involved in providing ore-forming materials for late Early Cretaceous Mo deposits in the SCMP.

(3) Regional petrological and geochemical data indicate that the late Early Cretaceous Mo mineralization took place in an extensional tectonic setting associated with the ongoing roll-back of the Paleo-Pacific slab.

Acknowledgments

This work is granted by the Postdoctoral Science Foundation of China (No. 2018M630203) and National Natural Science Foundation of China (Grant No. 41502090). The authors would like to thank Vice Editor Prof. Mao Jingwen, Dr. Liu Lian and two anonymous reviewers, who greatly improved discussion.

Manuscript received Aug. 1, 2018
accepted Dec. 20, 2018
associate EIC MAO Jingwen
edited by LIU Lian

References

Berzina, A.N., Sotnikov, V.I., Economou-Eliopoulos, M., and Eliopoulos, D.G., 2005. Distribution of rhenium in

molybdenite from porphyry Cu–Mo and Mo–Cu deposits of Russia (Siberia) and Mongolia. Ore Geology Review, 26(1–2): 91–113.

Chen, J., Foland, K.A., Xing, F., Xu, X., and Zhou, T., 1991. Magmatism along the southeastern margin of the Yangtze block: Precambrian collision of the Yangtze and Cathysia blocks of China. Geology, 19(8): 815–818.

Chen, P.R., Hua, R.M., Zhang, B.T., Lu, J.J., and Fan, C.F., 2002. Early Yanshanian post–orogenic granitoids in the Nanling region: Petrological constrains and geodynamic setting. Science in China (Series D), 45(8): 755–768.

Chen, Y.J., Wang, P., Li, N., Yang, Y.F., and Pirajno, F., 2017. The collision-type porphyry Mo deposits in Dabie Shan, China. Ore Geology Review, 81: 405–430.

Chen, J.Y., Yang, J.H., Zhang, J.H., Sun, J.F., and Wilde, S.A., 2013. Petrogenesis of the Cretaceous Zhangzhou batholith in southeastern China: Zircon U–Pb age and Sr–Nd–Hf–O isotopic evidence. Lithos, 162–163: 140–156.

Du, A.D., He, H.L., Yin, N.W., Zou, X.Q., Sun, Y.L., Sun, D.Z., Chen, S.Z., and Qu, W.J., 1995. A study of the rhenium-osmium geochronometry of molybdenites. Acta Geologica Sinica (English Edition), 8(2): 171–181.

Du, A.D, Wu, S.Q., Sun, D.Z., Wang, S.X., Qu, W.J., Stein, R.M.H., Morgan, J., and Malinovskiy, D., 2007. Preparation and Certification of Re–Os Dating Reference Materials: Molybdenite HLP and JDC. Geostandards and Geoanalytical Research, 28(1): 41–52.

Gan, X.C., Li, H.M., Sun, D.Z., Jin, W.S., and Zhao, F.Q., 1995. A geochronological study on Early Proterozoic granitic rocks, southwestern Zhejiang. Acta Petrologica et Mineralogica, 14 (1): 1–8 (in Chinese with English abstract).

Hoskin, P.W.O., and Schaltegger, U., 2003. The composition of zircon and igneous and metamorphic petrogenesis. Reviews in Mineralogy and Geochemistry, 53(1): 27–62.

Hu, L.S., Du, Y.S., Xu, Y.J., Wang, Z.W., and Wang, C.H., 2018. New Zircon U-Pb Age of Late Devonian Tuff in Guangxi, South China and the Significance for the Paleo-Tethys Branch Ocean. Acta Geologica Sinica (English Edition), 92(1): 402–403.

Jiang, Y.H., Zhao, P., Zhou Q., Liao S.Y., and Jin G.D., 2011. Petrogenesis and tectonic implications of Early Cretaceous S- and A-type granites in the northwest of the Gan-Hang rift, SE China. Lithos, 121(1–4): 55–73.

Li, Z.X., and Li, X.H., 2007. Formation of the 1300–km–wide intracontinental orogen and postorogenic magmatic province in Mesozoic South China: A flat-slab subduction model. Geology, 35(2): 179–182.

Li, X.H., Liu, Y., Li, Q.L., Guo, C.H., and Chamberlain, K.R., 2009. Precise determination of Phanerozoic zircon Pb/Pb age by multi-collector SIMS without external standardization. Geochemistry Geophysics Geosystems, 10(6): 1–21.

Li, Z.X., Li, X.H., Wartho, J.A., Clark, C., Li, W.X., Zhang, C.L., and Bao, C., 2010. Magmatic and metamorphic events during the early Paleozoic Wuyi-Yunkai orogeny, southeastern South China: New age constraints and pressure–temperature conditions. GSA Bulletin, 122(5–6): 772–793.

Li, J.H., Zhang, Y.Q., Dong, S.W., and Johnston, S.T., 2014. Cretaceous tectonic evolution of South China: A preliminary synthesis. Earth-Science Reviews, 134: 98–136.

Li, N., and Pirajno, F., 2017. Early Mesozoic Mo mineralization in the Qinling Orogen: An overview. Ore Geology Review, 81: 431–450.

Li, Q.Z., Yao, J.M., and Zhang, R.Q., 2018. Cassiterite U–Pb Date of the Yangbin Porphyry Tin. Acta Geologica Sinica (English Edition), 92(6): 2454–2456.

Liang, Q.L, Jiang, S.H., Wang, S.H., Li, C., and Zeng, F.G., 2012. Re–Os dating of molybdenite from the Luoboling porphyry Cu-Mo deposit in the Zijinshan ore field of Fujian province and its geological significance. Acta Geologica Sinica, 86(7): 1113–1118 (in Chinese with English abstract).

Lin, Z.Y., Wang, D.H., and Li, S.R., 2008. Re–Os isotope age of molybdenite from the Wangshe copper-tungsten deposit in Guangxi province and their implications. Acta Geologica Sinica, 82(11): 1565–1571 (in Chinese with English abstract).

Liu, Q., Yu, J.H., Wang, Q., Su, B., Zhou, M.F., Xu, H., and Cui, X., 2012. Ages and geochemistry of granites in the Pingtan–Dongshan Metamorphic Belt, Coastal South China: New constraints on late Mesozoic magmatic evolution. Lithos, 150: 268–286.

Ludwig, K.R., 2003. User's Manual for Isoplot 3.00, a geochronological Toolkit for Microsoft Excel. Berkeley Geochronology Center: Special Publication, 4: 25–32.

Mao, J.W., Zhang, Z.C., Zhang, Z.H., and Du, A.D., 1999. Re–Os isotopic dating of molybdenites in the Xiaoliugou W (Mo) deposit in the northern Qilian Mountains and its geological significance. Geochimica et Cosmochimica Acta, 63(11): 1815–1818.

Mao, J.W., Cheng, Y.B., Chen, M.H., and Franco, P., 2013. Major types and time-space distribution of Mesozoic ore deposits in South China and their geodynamic settings. Mineralium Deposita, 48(3): 267–294.

Mei, M.X., and Liu, S.F., 2017. The Late Triassic Sequence-Stratigraphic Framework of the Upper Yangtze Region, South China. Acta Geologica Sinica (English Edition), 91(1): 51–75.

Ni, P., Pan, J.Y., Wang, G.G., Chi, Z., Qin, H., Ding, J.Y., and Chen, H., 2017a. A CO_2-rich porphyry ore-forming fluid system constrained from a combined cathodoluminescence imaging and fluid inclusion studies of quartz veins from the Tongcun Mo deposit, South China. Ore Geology Review, 81: 856–870.

Ni, P., Wang, G.G., Cai, Y.T., Zhu, X.T., Yuan, H.Y., Huang, B., Ding, J.Y., and Chen, H., 2017b. Genesis of the Late Jurassic Shizitou Mo deposit, South China: Evidences from fluid inclusion, H–O isotope and Re–Os geochronology. Ore Geology Review, 81: 871–883.

Pirajno, F., Bagas, L., Hickman, A.H., and Team Gold Research, 1997. Gold mineralization of the Chencai-Suichang uplift and tectonic evolution of Zhejiang province, Southeast China. Ore Geology Review, 12(1): 35–55.

Qiu, J.S., Wang, D.Z., Mclnnes, B.I.A., Jiang, S.Y., Wang, R.C., and Kanisawa, S., 2004. Two subgroups of A-type granites in the coastal area of Zhejiang and Fujian Provinces, SE China: Age and geochemical constraints on their petrogenesis. Transactions of the Royal Society of Edinburgh Earth Sciences, 95(1–2): 227–236.

Qu, W.J., and Du, A.D., 2003. Highly precise Re–Os dating of molybdenite by ICP–MS with carius tube sample digestion. Rock and Mineral Analysis, 22(4): 253–262 (in Chinese with English abstract).

Smoliar, M.I., Walker, R.J., and Morgan, J.W., 1996. Re–Os ages of group IIA, IIIA, IVA and VIB iron meteorites. Science, 271 (5252): 1099–1102.

Shu, L.S., and Charvet, J., 1996. Kinematics and geochronology of the Proterozoic Dongxiang–Shexian ductile shear zone: with HP metamorphism and ophiolitic mélange (Jiangnan Region, South China). Tectonophysics, 267(1–4): 291–302.

Stein, H.J., Markey, R.J., Morgan, J.W., Du, A., and Sun, Y., 1997. Highly precise and accurate Re–Os ages for molybdenite from the East Qinling molybdenum belt, Shaanxi Province, China. Economic Geology, 92(7–8): 827–835.

Stein, H.J., Markey, R.J., Morgan, J.W., Hannah, J.L., and Schersten, A., 2001. The remarkable Re–Os chronometer inmolybdenite: how and why it works. Terra Nova, 13(6): 479–486.

Wang, C.H., Wang, D.H., Chen, Z.H., Yan, Z.H., Wu, Z.L., Lin, D.Y., and Liu, N.Z., 2009. Geological characteristics and metallogenic epoch of the Lishan molybdenite deposit-A discussion on regional prospecting for Mo in the Southeastern coast of China. Acta Mineralogica Sinica, 29(1): 64–69 (in Chinese with English abstract).

Wang, G.G., Ni, P., Zhao, C., Wang, X.L., Li, P.F., Chen, H., Zhu, A.D., and Li, L., 2016. Spatiotemporal reconstruction of Late Mesozoic silicic large igneous province and related epithermal mineralization in South China: Insights from the Zhilingtou volcanic–intrusive complex. Journal of Geophysical Research: Solid Earth, 121(11): 7903–7928.

Wang, Q., Wyman, D.A., Xu, J.F., Zhao, Z.H., Jian, P., Xiong, X.L., Bao, Z.W., Li, C.F., and Bai, Z.H., 2006. Petrogenesis of Cretaceous adakitic and shoshonitic igneous rocks in the Luzong area, Anhui Province (eastern China): Implications for

geodynamics and Cu–Au mineralization. Lithos, 89(3–4): 424–446.
Wang, Y.B., Zeng, Q.D., and Qu, W.J., 2013. Geological implications and Ages of three-stage Mo Polymetallic deposits, Zhejiang province. Acta Mineralogica Sinica, 29 (sup. 1): 55–56 (in Chinese).
Wang, Y.B., Zeng, Q.D., Liu, J.M., and Pirajno, F., 2017. Cretaceous magmatism and Mo mineralization in the South China Mo Province: U–Pb and Re–Os geochronology constraints from the Sanzhishu porphyry Mo deposit. Ore Geology Review, 81: 912–924.
Wang, Y.B., Zeng, Q.D., Zhang, S., Chen, P.W., and Gao, S., 2018. Spatial-temporal relationships of late Mesozoic granitoids in Zhejiang Province, Southeast China: constraints on tectonic evolution. International Geology Review, 60(11–14): 1529–1559.
Whitehouse, M.J., Kamber, B.S., and Moorbath, S., 1999. Age significance of U–Th–Pb zircon data from early Archaean rocks of west Greenland: A reassessment based on combined ion-microprobe and imaging studies. Chemical Geology, 160 (3): 201–224.
Wiedenbeck, M., Alle, P., Corfu, F., Griffin, W.L., Meier, M., Oberli, F., Vonquadt, A., Roddick, J.C., and Speigel, W., 1995. Three natural zircon standards for U–Th–Pb, Lu–Hf, trace-element and REE analyses. Geostandards Newsletter, 19(1): 1–23.
Wu, G.M., and Yang, W.D., 1999. Geological characters and analysis of exploration perspective of Lingjiao molybdenum deposit. Geology of Zhejiang, 15(2): 40–49 (in Chinese with English abstract).
Wu, Y.B., and Zheng, Y.F., 2004. Genesis of zircon and its constraints on interpretation of U–Pb age. Chinese Science Bulletin, 49(15): 1554–1569.
Xu, X.B., Xue, D.J., Li, Y., Hu, P., and Chen, N.S., 2014. Neoproterozoic sequences along the Dexing-Huangshan fault zone in the eastern Jiannan orogeny, South China: Geochronological and geochemical constraints. Gondwana Research, 25(1): 368–382.
Yang, S.Y., Jiang, S.Y., Zhao, K.D., Jiang, Y.H., Ling, H.F., and Luo, L., 2012. Geochronology, geochemistry and tectonic significance of two Early Cretaceous A-type granites in the Gan–Hang Belt, Southeast China. Lithos, 150: 155–170.
Zeng, Q.D., Wang, Y.B., Zhang, S., Liu, J.M., Qin, K.Z., Yang, J.H., Sun, W.D., and Qu, W.J., 2012. U–Pb and Re–Os geochronology of the Tongcun molybdenum deposit and Zhilintou gold-silver deposit in Zhejiang province, Southeast China, and its geological implications. Resource Geology, 63 (1): 99–109.
Zeng, Q.D., Liu, J.M., Qin, K.Z., Fan, H.R., Chu, S.X., Wang, Y.B., and Zhou, L.L., 2013. Types, characteristics, and time–space distribution of molybdenum deposits in China. International Geology Review, 55(11): 1311–1358.
Zhang, D.Q., Li, D.X., Feng, C.Y., and Dong, Y.J., 2001. The temporal and spatial framework of the Mesozoic magmatic system in Zijinshan area and its geological significance. Acta Geoscientia Sinica, 22(5): 403–408 (in Chinese with English abstract).
Zhang, K.Y., Wang, J.P., Du, A.D., Lin, Q.T., Huang, J.M., Hu, R.H., and Huang, Q.M., 2009. Re–Os isotopic dating of molybdenite from the Chilu molybdenite deposit in Fu'an, Fujian province. Geology in China, 36(1): 147–159 (in Chinese with English abstract).
Zhao, H.J., Zheng, W., Yu, C.F., Hu, Y.G., and Tian, Y., 2012. Re–Os dating of molybdenite from the Shilu Cu (Mo) deposit in western Guangdong province and its geological implications. Geology in China, 39(6): 1604–1613 (in Chinese with English abstract).
Zhao, Z.B., Xu, Z.Q., Ma, X.X., Liang, F.H., and Guo, P., 2018. Neoproterozoic–Early Paleozoic tectonic evolution of the South China Craton: New insights from the polyphase deformation in the southwestern Jiangnan Orogen. Acta Geologica Sinica (English Edition), 92(5): 1700–1727.
Zheng, Y.F., Xiao, W.J., and Zhao, G.C., 2013. Introduction to tectonics of China. Gondwana Research, 23(4): 1189–1206.
Zheng, W., Mao, J.W., Pirajno, F., Zhao, H.J., Zhao, C.S., Mao, Z.H., and Wang, Y.J., 2015. Geochronology and geochemistry of the Shilu Cu–Mo deposit in the Yunkai area, Guangdong Province, South China and its implication. Ore Geology Review, 67: 382–398.
Zhong, J., Chen, Y.J., and Pirajno, F., 2017. Geology, geochemistry and tectonic settings of the molybdenum deposits in South China: A review. Ore Geology Review, 81: 829–855.
Zhou, X., Li, W., 2000. Origin of Late Mesozoic igneous rocks in Southeastern China: Implications for lithosphere subduction and underplating of mafic magmas. Tectonophysics, 326(3–4): 269–287.
Zhou, X.M., Sun, T., Shen, W.Z., Shu, L.S., and Niu, Y.L., 2006. Petrogenesis of Mesozoic granitoids and volcanic rocks in South China: A response to tectonic evolution. Episodes, 29 (1): 26–33.
Zhu, K.Y., Li, Z.X., Xu, X.S., and Wilde, S.A., 2013. Late Triassic melting of a thickened crust in southeastern China: Evidence for flat-slab subduction of the paleo-Pacific plate. Journal of Asian Earth Sciences, 74(18): 265–279.

About the first and corresponding author

WANG Yongbin, male, born in 1985 in Xingtai City, Hebei province; Ph.D.; graduated from College of Earth and Planetary Sciences, University of Chinese Academy of Sciences; postdoctor at the Institute of Geology and Geophysics, Chinese Academy of Sciences. He is interested in porphyry-epithermal system. Email: wangyongbin@mail.iggcas.ac.cn; phone: 010-82998179.